

3D-Fingerprint Augment based on Super-Resolution for Indoor 3D WiFi Localization

Zhaoni Liu*, Xianmin Wang*, Zhikun Chen*, Ming Zhao*, Sihai Zhang*, Jingyue Li†

*Key Laboratory of Wireless-Optical Communications,

University of Science & Technology of China, Hefei, Anhui, P.R. China

† Department of Computer Science, Norwegian University of Science and Technology, Norway

Email: {znliu, wxm006, zhikunch}@mail.ustc.edu.cn, {zhaoming, shzhang}@ustc.edu.cn, jingyue.li@ntnu.no

Abstract—Recently, 3D indoor positioning technology has attracted wide attention in smart medical treatment, intelligent robot and other application fields. Traditional 3D positioning technology requires to utilize the special-dedicated infrastructure for large-scale deployment but with high labor-cost. With advent of the high-density wireless networks deployment, WiFi fingerprint-based localization system reduces the high cost of large-scale device deployment and infrastructure, but is limited by heavy site survey in the offline phase. Meanwhile, most existing WiFi fingerprint-based localization systems are only aimed at 2D indoor scenes. Designing and implementing a high-precision and low-cost 3D indoor positioning system is still a challenging task. Inspired by our previous work in fingerprint augment method based on super-resolution (FASR), we design the super-resolution (3D-FASR) framework and develop a novel 3D fingerprint augment method in this paper. The 3D-fingerprint augment technology in the 3D indoor environment has achieved an attractive trade-off between positioning accuracy, equipment deployment costs and site survey labor costs. We first obtain 2D fingerprint data from the 3D fingerprint data by slicing operations and then adopt FASR twice to complete the conversion from sparse fingerprint to dense fingerprint, where we interspersed a subsampling operation between two super-resolution methods. The experimental results demonstrate the feasibility of our proposed solution in 3D indoor localization.

Index Terms—3D, indoor WiFi localization, fingerprint augment, super-resolution, sparse reconstruction, low cost.

I. INTRODUCTION

Wireless localization technology has become a key driving factor for location-based services in a wide range of applications. 3D (3 Dimensions) indoor positioning relies on multi-dimensional positioning information to enhance its ability to empower applications, such as service-oriented localization and navigation, unmanned aircraft positioning, intelligent home, intelligent medical care and intelligent robotics [1]–[3]. Recently, 3D indoor positioning has been recognized by the Standardization Committee as an important aspect of wireless indoor positioning. e.g., Federal Communications Commission (FCC) [1] [4].

3D indoor localization can be defined as 3D locations determination relative to nearby reference points with known location in an interested indoor space. Traditionally, 3D indoor positioning based on ultra-wideband (UWB) technology can use measurement information such as time of arrival (TOA) or time difference of arrival (TDOA) [4]–[6] to locate the target. Due to the requirement of extremely high sampling rate

and strict time-synchronization between UWB transceivers, it is difficult to widely deploy and apply the traditional 3D indoor positioning in reality. In addition, radio frequency identification devices (RFIDs) can be attached to the target object for 3D localization with a larger-scale deployment [7]–[9]. In indoor scenarios, complex multipath propagation will severely weaken RFID signal, the positioning system provides low location accuracy. To our best knowledge, existing 3D localization systems are either limited by the special-dedicated infrastructures or poor location accuracy, which results in high cost, and thus make them unattractive in commercial applications. Therefore, how to design and implement a 3D localization system with low infrastructure cost while ensuring high location accuracy is still a challenging task.

Fortunately, with the development of the big data application of basic network [10] and the wide deployment of WiFi equipment, the WiFi fingerprint-based indoor positioning system becomes high-profile owing to its low cost of materials [11] and high location accuracy. Such a system usually includes two stages: offline and online phases [2]. Specifically, the fingerprint database is constructed in the offline phase. While in online phase, the positioning algorithm gives the localization result by comparing the received signal strength (RSS) vector collected at the unknown location with the fingerprint database. However, the offline RSS acquisition usually requires a lot of labor-cost [12]. Therefore, reducing the density of field investigation is the development direction of fingerprint-based positioning system. Existing solutions fall into two main categories. One is based on user participation, the tedious investigation into a small portion of each relevant user reasonable work, such as explicit data collection based on crowdsourcing [13], implicit data collection [14], and partially-labeled fingerprints [15]. The other is to increase the number of fingerprints by interpolation algorithm based on the collected sparse fingerprint data to reduce the acquisition cost, which is the so-called fingerprint augment [16]. Fingerprint augment is used more widely than user engagement based solutions, not only for general fingerprint data collection, but also in combination with user engagement categories.

The existing wireless fingerprint augment methods either adopt a propagation model [17] or regression estimation [18]. RSS estimation methods based on propagation models attempt to estimate RSS in non-line-of-sight (NLOS) regions

to create virtual fingerprints through propagation models. However, getting accurate virtual fingerprints is not easy to adapt to different environments and indoor layouts. The RSS estimation method based on regression uses the collected RSS data to calculate the parameters of the regression model, and then realizes the RSS estimation in each position. Gaussian Process Regression (GPR) [19] is the most common fingerprint augment method based on regression. Due to its various forms of mean function and covariance function, this method is precarious. Existing works like [20], [21] have discussed the design of these two functions, but it is difficult to find the optimal functional form of fingerprint augment. At present, the fingerprint augment challenge is how to find the optimal mapping function between the original sparse fingerprint database and augmented dense fingerprint database.

Single image super-resolution aims at reconstructing high resolution image from a single low resolution image [22]. Recently, the super resolution based on deep neural network has achieved remarkable results [23]. Inspired by the nonlinear mapping ability of deep neural network in image super-resolution, Wang et al. [24] innovatively introduce the super-resolution in image processing into indoor WiFi fingerprint augment and design the *Fingerprint-To-Image* conversion method to transform the WiFi fingerprint database into fingerprint images. Their numerical simulations and comparative experiments on the test platform verified the improved fingerprint enhancement and positioning accuracy.

Motivated by the FASR in 2D indoor localization, we proposed a **3D fingerprint augment** framework based on **super-resolution** (3D-FASR) for indoor 3D WiFi localization. Except for the existing FASR, there are three key components designed in our 3D-FASR, including *Slicing*, *Reconstruction* and *Decimation* (detailed in Section II).

The main contribution of this paper is, we innovatively propose the 3D-FASR to perform the 3D fingerprint augment based on the FASR for 3D indoor positioning. We then conduct the extensive experiments in numeric simulation to validate the performance improvement of fingerprint augment error and localization accuracy brought by the 3D-FASR.

II. THE 3D-FASR FRAMEWORK AND IMPLEMENTATION

Fig. 1 shows the proposed 3D-FASR framework, which comprises the following four modules. The *Slicing* module describes the generation of 2D-fingerprint slice database from the 3D-fingerprint database. The *FASR* module explains the super-resolution based 2D fingerprint augment, which finishes 2D-fingerprint super-resolution from sparse fingerprint data to dense fingerprint data. The *Reconstruction* module interprets the reconstruction of 3D-fingerprint database from the 2D-fingerprint database which can be considered as the reverse process of the *Slicing*. The *Decimation* module describes the downsampling process of the 3D-fingerprint matrix in a specific selected direction.

Fingerprint-based localization approaches employ a fingerprint database to record the RSS measurements. In a typical indoor 3D localization scheme, suppose there are a set of K

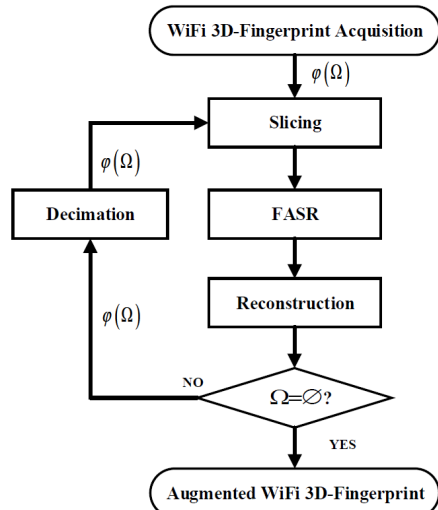


Fig. 1: The 3D-FASR Framework. (here the set Ω is initialized as $\Omega = \{X \text{ axis}, Y \text{ axis}, Z \text{ axis}\}$, the function $\phi(\Omega)$ is defined as operations which randomly select the direction ω from Ω and updates the $\Omega = \Omega - \{\omega\}$)

WiFi access points (APs) in several fixed positions, where the monitoring area is equally divided into G location grids. We can collect the RSS values of K APs on the G grids during a period of T consecutive timestamps, which further form the so called RSS 3D-fingerprint matrices \mathbf{R} , whose element can be expressed as

$$\mathbf{r} \in \mathbb{R}^{l \times m \times n}, \quad (1)$$

where l, m and n represent the number of grid in X axis, Y axis and Z axis directions of indoor 3D localization scenario, respectively. The index of element in \mathbf{r} represents the relative position of the 3D indoor space, while the RSS of the corresponding location is denoted by the value of element. Therefore, the 3D-fingerprint database \mathbf{R} contains $K \times T$ fingerprint matrices \mathbf{r} .

A. Slicing

In order to apply the FASR into our proposed 3D-FASR, we first need to acquire 2D-fingerprint database from 3D-fingerprint database. The above procedure is completed by slicing, i.e., it first selects a specific coordinate axis, cross-cuts the 3D matrices according to a certain granularity along the coordinate axis, and finally obtains the 2D matrices. Here the slicing operations and the generated 2D fingerprint databases along X, Y, Z axis are denoted by $\mathbf{g}_X, \mathbf{g}_Y, \mathbf{g}_Z$ and $\mathbf{S}_X, \mathbf{S}_Y$ and \mathbf{S}_Z , respectively .

Each 2D-fingerprint matrix belonging to the database can be expressed by $s_x \in \mathbb{R}^{m \times n}, s_y \in \mathbb{R}^{l \times n}$ and $s_z \in \mathbb{R}^{l \times m}$. Then, we have

$$\mathbf{g}_X : R \xrightarrow{X} S_X, \quad (2)$$

$$\mathbf{g}_Y : R \xrightarrow{Y} S_Y, \quad (3)$$

$$\mathbf{g}_Z : R \xrightarrow{Z} S_Z. \quad (4)$$

In our 3D-FASR framework, $\mathbf{S}_X, \mathbf{S}_Y$ and \mathbf{S}_Z representing the sparse 2D-fingerprint database will be fed into FASR to acquire super-resolution.

B. FASR

FASR framework is proposed to finish super-resolution recovery of 2D-fingerprint data based on EDSR networks. For more details, please refer to [24].

In our work, we assign coordinates for newly generated reference points (RPs) in dense database \mathbf{R}_{HR} according to the sparse database \mathbf{R}_{LR} . The RPs are uniformly distributed along the X axis, Y axis, Z axis directions and the distances of adjacent RPs over each directions are consistent. We denote the minimum distance of different RPs in \mathbf{R}_{LR} and \mathbf{R}_{HR} as λ_{LR} and λ_{HR} . Then we can describe the factor of fingerprint augment by μ

$$\mu = \frac{\lambda_{LR}}{\lambda_{HR}}, \quad (5)$$

Clearly, if the grid numbers in the X axis direction under the sparse condition are l , then the grid numbers in this direction of the enhanced dense fingerprint are μl .

Before the 3D-FASR, we separately generate three different axes training slice database to finish the train of FASR, in which the factor of fingerprint augment is set as μ . Then we can obtain different directional super-resolution augment networks denoted by X-FASR, Y-FASR and Z-FASR.

In the 3D-FASR, we choose and feed the slice databases S_X, S_Y and S_Z into X-FASR, Y-FASR and Z-FASR, respectively. Then, we can separately acquire the same amount of augmented 2D fingerprint databases denoted by S'_X, S'_Y and S'_Z , and each 2D-fingerprint matrix belonging to the database can be expressed by $s'_x \in \mathbb{R}^{\mu m \times \mu n}, s'_y \in \mathbb{R}^{\mu l \times \mu n}$ and $s'_z \in \mathbb{R}^{\mu l \times \mu m}$. The processing can be represented as

$$\text{X-FASR} : S_X \longrightarrow S'_X, \quad (6)$$

$$\text{Y-FASR} : S_Y \longrightarrow S'_Y, \quad (7)$$

$$\text{Z-FASR} : S_Z \longrightarrow S'_Z. \quad (8)$$

After this, we can obtain the augmented 2D-fingerprint databases along different axes, which are further used for 3D fingerprint reconstruction.

C. Reconstruction

In order to make sure a correct dimension of the output in our solution, the reconstruction from 2D to 3D fingerprint is needed. Thus, to reverse the process of slicing, we reconstruct the augmented 3D-fingerprint database from the augmented 2D-fingerprint database. The reconstruct operations and 3D-fingerprint databases along X, Y, Z axis are respectively denoted by $\mathbf{g}'_X, \mathbf{g}'_Y, \mathbf{g}'_Z$ and $\mathbf{R}'_X, \mathbf{R}'_Y$ and \mathbf{R}'_Z . Each 3D-fingerprint matrix belonging to the database can be expressed by $r_x \in \mathbb{R}^{l \times \mu m \times \mu n}, r_y \in \mathbb{R}^{\mu l \times m \times \mu n}$ and $r_z \in \mathbb{R}^{\mu l \times \mu m \times n}$. The reconstruction processes are recorded as

$$\mathbf{g}'_X : S'_X \xrightarrow{X} \mathbf{R}'_X, \quad (9)$$

$$\mathbf{g}'_Y : S'_Y \xrightarrow{Y} \mathbf{R}'_Y, \quad (10)$$

$$\mathbf{g}'_Z : S'_Z \xrightarrow{Z} \mathbf{R}'_Z. \quad (11)$$

After the reconstruction, the obtained reconstructed 3D-fingerprints are put into the Decimation.

D. Decimation

After the above three modules, it accomplishes the 2D fingerprint augmentation of pre-selected axis vertical section. Nevertheless, the number of pre-selected axis directional RPs is remain unchanged. To address it, a feasible way is to perform the above steps again. To meet the requirement of the second FASR, we arbitrarily choose another direction which is different from the already selected axis in the first time to perform decimation, and deal with the 3D-fingerprint database by downsampling factor μ . The new 3D-fingerprint matrix belonging to three different axes directions are denoted by $r_{x1} \in \mathbb{R}^{l \times m \times \mu n}$ or $r_{x2} \in \mathbb{R}^{l \times \mu m \times n}$ (if X axis is selected for the first FASR), $r_{y1} \in \mathbb{R}^{l \times m \times \mu n}$ or $r_{y2} \in \mathbb{R}^{\mu l \times m \times n}$ (if Y axis is selected for the first FASR), $r_{z1} \in \mathbb{R}^{l \times \mu m \times n}$ or $r_{z2} \in \mathbb{R}^{\mu l \times m \times n}$ (if Z axis is selected for the first FASR).

When the decimation operation is accomplished, we should select the remaining axis directions and dispose them sequentially by slicing, FASR and reconstruction for the second time. In the practical implementation of 3D-FASR, we can select the order direction of the axis in advance, so that only two given FASR networks can be trained to reduce the workload.

After the above modules, 3D-FASR accomplishes the conversion from the 3D-fingerprint matrices $\mathbf{r} \in \mathbb{R}^{l \times m \times n}$ to dense 3D-fingerprint matrices $\mathbf{r}_{HR} \in \mathbb{R}^{\mu l \times \mu m \times \mu n}$.

III. EXPERIMENTAL RESULTS AND EVALUATION

In this section, the proposed 3D-FASR is verified in a simulated scenario, and the performance of fingerprint augment and localization are presented and discussed. In our implementation, we sequentially select the Z axis, Y axis and X axis. The downsampling factor of the FASR in super-resolution is set as $\mu = 3$. As for the baseline, we select the basic GPR (B-GPR) [25] with zero-mean function and squared exponential kernel covariance function [20] for fingerprint augment comparison. This paper adopts standard weighted k-nearest neighbor (WKNN) as localization algorithm [21].

A. Experimental Settings

In localization scenario, the space has a volume $8m \times 8m \times 8m$, 7 APs with fixed locations are posted, a total number of 3,375 RPs are divided with $\lambda_{HR} = 0.5m$ and each direction has $l = m = n = 15$ grid points, the position indexes on the correlation axis are $0.5 : 0.5 : 7.5$ ¹.

Time-invariant multipath channels are used to obtain experimental data [26] and RSS values from APs are generated

¹Here the $0.5 : 0.5 : 7.5$ represents for the geo-distribution of RPs in the room. The three parameters represent the left endpoint, the sampling interval and the right endpoint values, respectively. $0.5 : 0.5 : 7.5$ equals to $[0.5, 1.0, 1.5, 2.0, 2.5, 3.0, 3.5, 4.0, 4.5, 5.0, 5.5, 6.0, 6.5, 7.0, 7.5]$

using raytracing technology [27]. For each AP, the RSS value at each location is obtained by superposing the signal from a direct path and six signals reflected from the walls. The Log-Distance path loss model in free space is used to calculate the RSS value of each path.

For the training dataset, we simulate the generation of fingerprint data matrix with $T=3,000$ different timestamps. Since 7 APs are placed in the localization scene, we could obtain 7 3D-fingerprint matrices at each timestamp, which comprises a total of 21,000 3D-fingerprint matrices of $\lambda_{HR} = 0.5m$, i.e., the training data. For simulated scenario, the 21,000 3D-fingerprint matrices with $\lambda_{HR} = 0.5m$ are seen as the R , the size of each 3D-fingerprint matrix in the R is $15 \times 15 \times 15$. We generate different directional slice database S_X, S_Z by (2)(4), which are used as the ground truth. The dataset in each direction contains $21,000 \times 15 = 315,000$ 2D-fingerprint matrices with size 15×15 .

While for the test dataset, we generate fingerprint data with $\lambda_{HR} = 0.5m$ and $T = 100$ to form a test set. Each segment of RPs is extracted with $\lambda_{LR} = 1.5m$ to build a sparse WiFi fingerprint database. The sparse 3D-WiFi fingerprint database is converted into 7 low-resolution fingerprint matrix, where $\lambda_{LR} = 1.5m$ and the super-resolution is I_{HR} . In addition, 1,000 location test points are randomly selected to evaluate the performance of the localization.

B. 3D-FASR Training

In this phase, we use 15×15 fingerprint matrix and set the $\mu = 3$ to obtain the 5×5 low-resolution fingerprint matrix with $\lambda_{LR} = 1.5m$ and the corresponding 15×15 high-resolution fingerprint matrix with $\lambda_{HR} = 0.5m$. We train the FASR network with ADAM optimizer [22] and set minibatch size as 100.

C. Performance of Fingerprint Augment

As for fingerprint augment performance, the RSS estimation error e_t of t -th segment is defined as follows

$$e_t = \frac{1}{l \times m \times n} \sum_{k=1}^l \sum_{j=1}^m \sum_{i=1}^n |R_{i,j,k}^t - R_{i,j,k}'^t|, \quad (12)$$

where $R_{i,j,k}^t, R_{i,j,k}'^t$ respectively denotes the original RSS value and the augmented RSS value in coordinates (i, j, k) . Fig. 2 shows the error of fingerprint augment using 3D-FASR and B-GPR in simulated scenarios.

TABLE I: Comparison of RSS Augmentation Errors (dBm).

Simulate	3D-FASR	B-GPR
mean	1.005600	1.569000
var	0.000019	0.073289

As shown in Fig. 2, when comparing with B-GPR, 3D-FASR has the smaller error of fingerprint augment. Meanwhile, the experimental result also shows that B-GPR is not robust, and the performance is less stable than 3D-FASR.

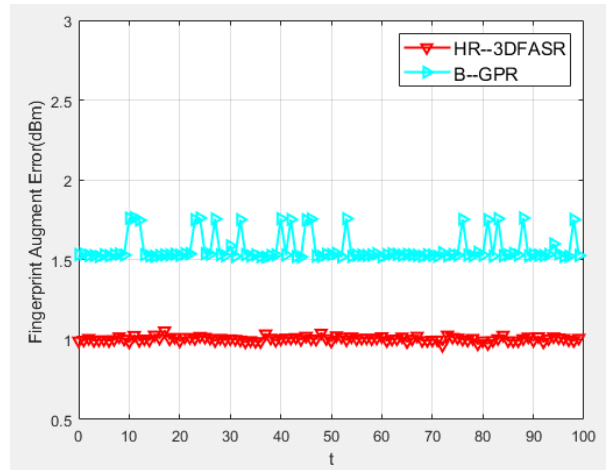


Fig. 2: Performance comparison of fingerprint augment (3D-FASR, B-GPR).

TABLE II: Comparison of Average Localization Errors (m).

Simulate	LR	HR-ORIG	3D-FASR	B-GPR
mean	1.4152	1.0271	1.1237	1.1919
var	0.6896	0.4600	0.4846	0.5485

To better demonstrate the fingerprint augment performance, we also compare the mean value and variance of the RSS augmented by our 3D-FASR with that by B-GPR, which is shown in TABLE I. Clearly, we can see that our solution gets a smaller mean value and variance comparing to B-GPR, which suggests that our solution harvests a better fingerprint augmentation performance.

D. Performance of Localization

As for localization performance, the localization error e_i^L of i -th positioning test points is defined as follows

$$e_i^L = \|S_i - S_i'\|_2, \quad (13)$$

where S_i and S_i' represent the real physical position and the estimation location. The cumulative distribution function (CDF) for location error is shown in Fig. 3. We can find that 3D-FASR is obviously better than B-GPR and has a closer localization performance to HR-ORIG. In addition, the localization performance after fingerprint augment is better than LR, which further indicates the effectiveness of fingerprint augment.

Similarly, we also calculate the mean and variance of the positioning error and show them in Tabel II. In the experiment, 3D-FASR performs better than B-GPR and LR with its average localization error 5.71% lower than B-GPR and 20.5% lower than LR, and the stability of 3D-FASR's localization performance is only slightly worse than to HR-ORIG. With the only 1/27 cost of manual acquisition comparing to the HR-ORIG, we can get an acceptable localization performance of 3D-FASR which is only 9.4% lower than the performance of ORIG.

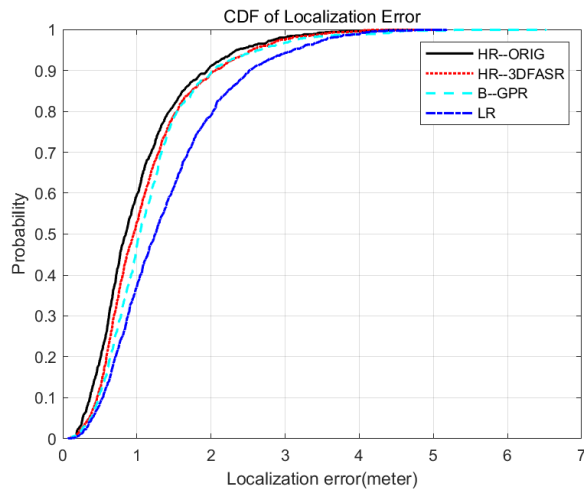


Fig. 3: Performance comparison of localization. ‘LR’ means the positioning result without fingerprint augment. ‘HR-ORIG’ means the original dense fingerprint database obtained by simulation. The others represent the localization results of the augmented fingerprint database which is constructed by 3D-FASR and B-GPR.

IV. CONCLUSION

In order to improve the accuracy of 3D indoor localization based on WiFi fingerprint under the condition of limited fingerprint and workload of on-site measurement, we propose a 3D-FASR solution in this work. To verify the performance of 3D-FASR, we carry out the experiments in the simulation scene, and compare the RSS augmentation and positioning accuracy of our solution with B-GPR. The experimental results confirm the effectiveness of 3D-FASR in improving fingerprint augment and localization accuracy.

ACKNOWLEDGMENT

This work was partially supported by Key Program of Natural Science Foundation of China under Grant (61631018), Huawei Technology Innovative Research (YBN2018095087).

REFERENCES

- [1] A. Yassin, Y. Nasser, M. Awad, A. Al-Dubai, R. Liu, C. Yuen, and R. Raulefs, “Recent advances in indoor localization: A survey on theoretical approaches and applications,” *IEEE Communications Surveys & Tutorials*, vol. PP, pp. 1–11, 2016.
- [2] M. Youssef, A. Agrawala, and A. Udaya Shankar, “Wlan location determination via clustering and probability distributions,” in *Proceedings of the First IEEE International Conference on Pervasive Computing and Communications, 2003. (PerCom 2003)*, 2003, pp. 143–150.
- [3] H. Liu, H. Darabi, P. Banerjee, and J. Liu, “Survey of wireless indoor positioning techniques and systems,” *IEEE Transactions on Systems Man & Cybernetics Part C*, vol. 37, no. 6, pp. 1067–1080, 2007.
- [4] C. Meier, A. Terzis, and S. Lindenmeier, “A robust 3d high precision radio location system,” in *2007 IEEE/MTT-S International Microwave Symposium*. IEEE, 2007, pp. 397–400.
- [5] M. R. Mahfouz, C. Zhang, B. C. Merkl, M. J. Kuhn, and A. E. Fathy, “Investigation of high-accuracy indoor 3-d positioning using uwb technology,” *IEEE Transactions on Microwave Theory & Techniques*, vol. 56, no. 6, pp. 1316–1330, 2008.
- [6] C. Zhang, M. Kuhn, B. Merkl, M. Mahfouz, and A. E. Fathy, “Development of an uwb indoor 3d positioning radar with millimeter accuracy,” in *2006 IEEE MTT-S International Microwave Symposium Digest*, 2006, pp. 106–109.

- [7] J. Maneesilp, C. Wang, H. Wu, and N. F. Tzeng, “Rfid support for accurate 3d localization,” *IEEE Transactions on Computers*, vol. 62, no. 7, pp. 1447–1459, 2013.
- [8] C. Wang, H. Wu, and N.-F. Tzeng, “Rfid-based 3-d positioning schemes,” in *IEEE INFOCOM 2007-26th IEEE International Conference on Computer Communications*. IEEE, 2007, pp. 1235–1243.
- [9] L. M. Ni, Y. Liu, Y. C. Lau, and A. P. Patil, “Landmarc: Indoor location sensing using active rfid,” in *Proceedings of the First IEEE International Conference on Pervasive Computing and Communications, 2003. (PerCom 2003)*. IEEE, 2003, pp. 407–415.
- [10] P. Lu, L. Zhang, X. Liu, J. Yao, and Z. Zhu, “Highly efficient data migration and backup for big data applications in elastic optical inter-data-center networks,” *IEEE Network*, vol. 29, no. 5, pp. 36–42, 2015.
- [11] K. Lin, M. Chen, J. Deng, M. Hassan, and G. Fortino, “Enhanced fingerprinting and trajectory prediction for iot localization in smart buildings,” *IEEE Transactions on Automation Science and Engineering*, vol. 13, no. 3, pp. 1294–1307, 2016.
- [12] J. Xiao, Z. Zhou, Y. Yi, and L. Ni, “A survey on wireless indoor localization from the device perspective,” *ACM Computing Surveys*, vol. 49, no. 2, p. 25, 2016.
- [13] J. Ledlie, J. Park, D. Curtis, A. Cavalcante, L. Camara, A. Costa, and R. Vieira, “Molé: a scalable, user-generated wifi positioning engine,” *Journal of Location Based Services*, vol. 6, no. 2, pp. 55–80, 2012.
- [14] C. Luo, H. Hong, and M. C. Chan, “Piloc: A self-calibrating participatory indoor localization system,” in *IPSN-14 Proceedings of the 13th International Symposium on Information Processing in Sensor Networks*, 2014, pp. 143–153.
- [15] S. Sorour, Y. Lostanlen, S. Valaee, and K. Majeed, “Joint indoor localization and radio map construction with limited deployment load,” *IEEE Transactions on Mobile Computing*, vol. 14, no. 5, pp. 1031–1043, 2014.
- [16] G. Caso, L. De Nardis, and M. Di Benedetto, “Low-complexity offline and online strategies for wi-fi fingerprinting indoor positioning systems,” in *Geographical and Fingerprinting Data to Create Systems for Indoor Positioning and Indoor/Outdoor Navigation*, 2019, pp. 129–145.
- [17] G. Caso and L. De Nardis, “On the applicability of multi-wall multi-floor propagation models to wifi fingerprinting indoor positioning,” in *Future Access Enablers of Ubiquitous and Intelligent Infrastructures*. Springer, 2015, pp. 166–172.
- [18] H. Zou, M. Jin, H. Jiang, L. Xie, and C. Spanos, “Winips: Wifi-based non-intrusive indoor positioning system with online radio map construction and adaptation,” *IEEE Transactions on Wireless Communications*, vol. 16, no. 12, pp. 8118–8130, 2017.
- [19] C. Rasmussen, “Gaussian processes in machine learning,” in *Summer School on Machine Learning*, 2003, pp. 63–71.
- [20] W. Sun, M. Xue, H. Yu, H. Tang, and A. Lin, “Augmentation of fingerprints for indoor wifi localization based on gaussian process regression,” *IEEE Transactions on Vehicular Technology*, vol. 67, no. 11, pp. 10896–10905, 2018.
- [21] X. Wang, T. Lan, S. Zhang, and J. Zhu, “Signal distribution oriented mean functions in gr based fingerprint augment,” in *2019 11th International Conference on Wireless Communications and Signal Processing (WCSP)*. IEEE, 2019, pp. 1–6.
- [22] B. Lim, S. Son, H. Kim, S. Nah, and K. Mu Lee, “Enhanced deep residual networks for single image super-resolution,” in *CVPR Workshops*, July 2017.
- [23] Z. Wang, J. Chen, and S. C. H. Hoi, “Deep learning for image super-resolution: A survey,” *IEEE Transactions on Pattern Analysis and Machine Intelligence*, vol. 43, no. 10, pp. 3365–3387, 2021.
- [24] X. Wang, Z. Chen, S. Zhang, and J. Zhu, “Super-resolution based fingerprint augment for indoor wifi localization,” in *GLOBECOM 2020 - 2020 IEEE Global Communications Conference*, 2020, pp. 1–6.
- [25] S. Yiu, M. Dashti, H. Claussen, and F. Perez-Cruz, “Wireless rssi fingerprinting localization,” *Signal Processing*, vol. 131, pp. 235–244, 2017.
- [26] Y. Qi and H. Kobayashi, “On relation among time delay and signal strength based geolocation methods,” in *IEEE Global Telecommunications Conference*, vol. 7. IEEE, 2003, pp. 4079–4083.
- [27] Z. Yun and M. Iskander, “Ray tracing for radio propagation modeling: Principles and applications,” *IEEE Access*, vol. 3, pp. 1089–1100, 2015.